Plcγ2/Tmem178 dependent pathway in myeloid cells modulates the pathogenesis of cytokine storm syndrome

Sahil Mahajan[a], Corinne E. Decker[a], Zhengfeng Yang[a], Deborah Veis[b], Elizabeth D. Mellins[c], Roberta Faccio[a,d,*]

[a] Department of Orthopaedic Surgery, Musculoskeletal Research Center, Washington University School of Medicine, St. Louis, MO, USA
[b] Division of Bone and Mineral Disease, Department of Medicine, Musculoskeletal Research Center, Washington University School of Medicine, St. Louis, MO, USA
[c] Department of Pediatrics, Program in Immunology, Stanford University, Stanford, CA, USA
[d] Shriners Hospitals for Children, St. Louis, MO, USA

ABSTRACT

Cytokine storm syndrome (CSS) is a life-threatening condition characterized by excessive activation of T cells and uncontrolled inflammation, mostly described in patients with familial hemophagocytic lymphohistiocytosis and certain systemic auto-inflammatory diseases, such as systemic juvenile idiopathic arthritis (sJIA). Defects in T cell cytotoxicity as a mechanism for uncontrolled inflammation following viral infections fail to represent the whole spectrum of CSS. Evidence implicates dysregulated innate immune responses, especially activation of monocytes and macrophages, in patients with CSS. However, the direct contribution of monocytes/macrophages to CSS development and the signaling pathways involved in their activation have not been formally investigated. We find that depletion of monocytes/macrophages during early stages of CSS development, by clodronate-liposomes or neutralizing anti-CSF1 antibody, reduces mortality and inflammatory cytokine levels in two CSS mouse models, one dependent on T cells and the second induced by repeated TLR9 stimulation. We further demonstrate that activation of Plcγ2 in myeloid cells controls CSS development by driving macrophage pro-inflammatory responses. Intriguingly, the Plcγ2 downstream effector Tmem178, a negative modulator of calcium levels, acts in a negative feedback loop to restrain inflammatory cytokine production. Genetic deletion of Tmem178 leads to pro-inflammatory macrophage polarization *in vitro* and more severe CSS *in vivo*. Importantly, Tmem178 levels are reduced in macrophages from mice with CSS and after exposure to plasma from sJIA patients with active disease. Our data identify a novel Plcγ2/Tmem178 axis as a modulator of inflammatory cytokine production by monocytes/macrophages. We also find that loss of Tmem178 accentuates the pro-inflammatory responses in CSS.

1. Introduction

Cytokine storm syndrome (CSS) is a severe, potentially fatal condition characterized by uncontrolled proliferation of T cells and macrophages, over production of inflammatory cytokines and accumulation of well-differentiated phagocytic macrophages that engulf other blood cells in the bone marrow [1]. CSS is associated with a wide variety of infectious and non-infectious diseases, including influenza [2], familial hemophagocytic lymphohistiocytosis [3], systemic juvenile idiopathic arthritis (sJIA) and Lupus [4], and has even been detected in cancer patients following chimeric antigen receptor (CAR)-T cell therapy [5,6]. Due to similarities with various inflammatory conditions, diagnostic and treatment delays can lead to a significant mortality rate [1,7–10].

The causes of CSS are still under investigation. Numerous studies focused on mutations in T cell cytotoxic pathways and the signals involved in T cell hyperactivity following viral infections [11–14]. However, there is substantial data pointing to a role for monocytes/macrophages in the etiology of CSS. Gene expression profiling of peripheral blood mononuclear cells obtained from untreated sJIA patients identified a cluster of genes more highly expressed in patients with high levels of ferritin, a marker of sub-clinical and clinical CSS, compared to untreated sJIA patients with normal ferritin [15]. This cluster included genes associated with innate immune responses, particularly those downstream of toll like receptor (TLR)/IL-1R signaling [15]. Furthermore, polymorphisms in the gene encoding the transcription factor interferon regulatory factor 5 (IRF5), activated downstream of TLR and

a marker of pro-inflammatory macrophages, are associated with increased susceptibility of developing CSS among sJIA patients [16,17]. Accumulation of monocytes and macrophages in spleen and liver and very high systemic levels of pro-inflammatory cytokines like IL-18, IL-6, and TNFα are commonly observed in CSS patients. Targeting IFNγ, which reduces the numbers of activated monocytes and macrophages, protects from development of CSS in mouse models [3,18–22]. High levels of inflammatory cytokines and chemokines produced by monocytes and macrophages are also detected in acute lymphoblastic leukemia patients developing CSS following treatment with CAR-T cell therapy [23]. Importantly, depletion of monocytes/macrophages prior to the administration of CAR-T cells significantly reduces the inflammation and its associated mortality in animal models [23,24]. Intriguingly, blockade of CCR2, which prevents the recruitment of inflammatory monocytes from the bone marrow to the peripheral tissues, has no protective effects in the TLR9-induced CSS mouse model; extramedullary monocytosis instead contributes to the expansion of monocytes in liver and spleen in these mice [21]. These clinical and preclinical observations suggest that hyperactivation of monocytes/macrophages might be an underlying cause of CSS initiation. In support of this hypothesis, not all CSS patients have genetic defects linked to aberrant T cell activation.

Animal models of CSS have been developed only in recent years based on the clinical features observed in the patients. Since episodes of CSS in familial hemophagocytic lymphohistiocytosis and sJIA patients appear to be most commonly triggered by viral infections often in association with genetic defects in T cell cytotoxic pathways, one of the most common mouse model utilizes Perforin-deficient (*Prf* − / −) mice infected with lymphocytic choriomeningitis virus (LCMV). Unlike wild type mice where LCMV incites a strong $CD8^+$ T cell response, *Prf* − / − develop a deleterious course after infection with LCMV due to defects in T cell cytotoxic responses against the virus which lead to accumulation of T cells and macrophage activation [11]. These mice develop splenomegaly, hepatomegaly, cytokinemia and hyperferritinemia and die within 3 weeks post-infection. All clinical features and associated mortality can be mitigated by the depletion of $CD8^+$ T cells or neutralization of IFNγ [11,25]. A second mouse model of CSS consisting of repeated injections of the TLR9 ligand CpG into wild-type mice was developed based on clinical evidence of persistently activated TLR signaling in some CSS patients. This model does not lead to lethality and the CSS-like clinical features cannot be prevented by T cell depletion [22]. Interestingly accumulation of monocytes and macrophages is observed in both animal models, but their direct contribution to CSS initiation/development and most importantly the signaling pathways involved in their activation have not been formally investigated.

In this study by using a combination of pharmacological and genetic approaches we demonstrate that targeting monocytes/macrophages limits CSS progression in two established CSS mouse models. We also find that Plcγ2 is required for monocyte/macrophage pro-inflammatory responses. Intriguingly, Plcγ2 also activates a negative feedback loop pathway to restrain inflammatory cytokine production via Tmem178, a negative modulator of intracellular calcium levels [26]. Our data identify a novel Plcγ2/Tmem178 axis as a driver of inflammation in CSS.

2. Materials and methods

2.1. Mice

C57Bl/6 *Tmem178* − / − mice obtained from the KOMP repository at the University of California Davis and WT mice are maintained by heterozygous breeding. C57Bl/6 Plcγ2$^{flox/flox}$ mice were obtained from T. Kurosaki (Kansai Medical University, Moriguchi, Japan [27]; and *Plcγ2*$^{flox/flox}$; LysM-Cre (*Plcγ2cKO*) mice were obtained via intercrossing *Plcγ2*$^{flox/flox}$ mice with LysM-Cre mice. *Prf* − / − mice were purchased from the Jackson Laboratory (Bar Harbor, ME) and *Prf* − /

− *Tmem178* − / − double knockout mice were obtained by intercrossing *Prf* − / − with *Tmem178* − / − mice. All experiments were approved by the Washington University School of Medicine animal care and use committee.

2.2. CpG-induced model of CSS

50 μg CpG 1826 (IDT) was injected intraperitoneally into 6 to 8 week-old male or female mice every 2 days. Because no differences between males and females were noted, we used mice of both sexes. On day 9, animals were bled via submandibular vein puncture for complete blood count and euthanized to collect organs. To deplete monocytes/macrophages, 100 μl of clodronate-liposomes (ClodronateLiposomes. org) were intravenously injected 2 days prior to the first CpG injection and 48 and 96 h later.

2.3. LCMV-induced model of CSS

2×10^5 plaque-forming units (PFUs) of LCMV-Armstrong were administered intraperitoneally in 8–12 week-old *Prf* − / − or *Prf-Tmem178* double knockout mice. To deplete monocytes/macrophages, 100 μl of clodronate-liposomes were intravenously injected into *Prf* − / − mice two days prior to the LCMV infection and 48 and 96 h later. Alternatively, 1 mg of the neutralizing anti-CSF1 antibody (Clone 5A1, BioXCell) was administered 2 days prior to infection, and 0.5 mg antibody was administered 48 and 96 h later. Animals were bled via submandibular vein puncture to measure serum cytokines on days 3 and 8 post-infection.

2.4. Liver processing for cell isolation

The mice were euthanized after the last CpG injection and livers were immediately harvested without perfusion and processed by chopping them into fine pieces followed by digestion with collagenase (Roche) and DNase I (Sigma) solution for 45 min at 37 °C. The tissue suspension was then filtered through a 70-μm cell strainer (MIDSCI) to obtain single-cell suspensions. Red blood cells were lysed in Red Blood Cell Lysis Buffer (Sigma), and the remaining cells were either stained with indicated antibodies and analyzed by flow cytometry, or subjected to sorting using MACS columns. In some circumstances, a small piece of liver tissue was lysed in Trizol for RT-qPCR analysis.

2.5. Flow cytometry

Single cell suspensions obtained from liver tissues as indicated in 2.4 were stained in FACS buffer with the following anti–mouse antibodies: PE-Cy5 conjugated anti-F4/80 (eBioscience), Alexa Fluor 700 conjugated anti-CD11b (eBioscience), PE-Cy7 conjugated anti-CD45 (eBioscience), FITC conjugated CD4 (BioLegend), BUV395 conjugated CD8a (BD Biosciences), Pacific Blue conjugated CD44 (BioLegend), FITC conjugated F4/80 (BioLegend), FITC conjugated CD3e (BD Biosciences), FITC conjugated Ly-6G (BioLegend), APC-eFluor 780 conjugated CD11c (eBioscience), APC conjugated IFNγ (BioLegend), PerCP-Cy5.5 conjugated Ly-6C (eBioscience) and PE conjugated anti-Ly6G (BioLegend). Acquisition was performed on a LSR Fortessa, LSR Fortessa X-20 or LSRII. Data were analyzed with FlowJo 7.5.5 software (Tree Star).

2.6. Magnetic activated cell sorting (MACS)

$CD11b^+$ and $F4/80^+$ cells were isolated after liver processing as described in 2.4 using the MACS kits according to the manufacturer's instructions (Miltenyi Biotech, CD11b: 130-049-601 and F4/80: 130-110-443). Briefly, 10^7 total cells obtained after enzymatic digestions of liver samples were incubated with either CD11b or F4/80 microbeads and subsequently added to the MACS column placed in the magnetic

field of a MACS separator (Miltenyi Biotech). The CD11b$^+$ and F4/80$^+$ cells were collected following manufacturer's instructions.

2.7. Quantitative RT-PCR

Total RNA was isolated with TRIzol reagent (Invitrogen) from either cells or liver samples using the RNeasy Mini Kit (Qiagen) and reverse transcribed to cDNA using High Capacity cDNA reverse transcription kit (Applied Biosystems) according to the manufacturer's instructions. For real-time PCR, SYBR Green PCR Master Mix (Applied Biosystems) and primers specific for murine Tmem178, IL-1β, IL-6, TNF-α, IL-10, iNOS, CCL5, IRF5, Arginase 1, PPARγ and cyclophilin were used as follow: for Tmem178, ATGACAGGGATATTTTGCACCAT (forward) and CCGGTTC AAGTCATAGGAGACACT (reverse); IL-1β, GCTTCCTTGTGCAAGTGTC TGA (forward) and TCAAAAGGTGGCATTTCACAGT (reverse); IL-6, TTCTCTGGGAAATCGTGGAAA (forward) and TGCAAGTGCATCATCG TTGTT (reverse); TNFα, CTGTAGCCCACGTCGTAGC (forward) and TTGAGATCCATGCCGTTG (reverse); iNOS, ACTCAGCCAAGCCCTCACC (forward) and GCCTATCCGTCTCGTCCGT (reverse); CCL5, AGATCTC TGCAGCTGCCCTCA (forward) and GGAGCACTTGCTGCTGGTGTAG (reverse); IRF5, TGTCCCAGACCCAAATCTCC (forward) and CTCTAGG TCCGTCAAAGGCA (reverse); Arginase 1, ATGGAAGAGACCTTCAGC TAC (forward) and GCTGTCTTCCCAAGAGTTGGG (reverse); PPARγ, ACTCATACATAAAGTCCTTCCCGCT (forward) and ATGGTGATTTGTC CGTTGTCTTTCC (reverse); IL-10, GATGCCCCAGGCAGAGAA (forward) and CACCCAGGGAATTCAAATGC (reverse) and for cyclophilin AGCA TACAGGTCCTGGCATC (forward) and TTCACCTTCCCAAAGACCAC-3' (reverse). SYBR green dye was used for detection of the product using the SYBR Green PCR Master Mix assay (Applied Biosystems). The relative abundance of each target was calculated as $2^{-(Ct\ target\ gene - Ct\ cyclophilin)}$, where Ct represents the threshold cycle for each transcript, and cyclophilin is the reference housekeeping gene. The fold change was determined by plotting $2^{-\Delta\Delta Ct}$ and by setting the expression of unstimulated BMMs to 1.

2.8. Measurement of cytokine levels

Cytokines and chemokines in cell culture supernatants or from serum were quantified using ELISA kits specific for IL-6, TNFα and IL-1β (eBioscience) or using MILLIPLEX kit (EMD MILLIPORE) following the manufacturer's instructions.

2.9. Calcium imaging

For calcium imaging 2×10^5 WT or *Tmem178*$-/-$ BMMs were plated in 29 mm glass bottom dishes, and adherent cells were incubated with 2 μM Fura-2-AM diluted in Hanks' Balanced Salt Solution (HBSS) containing 2 mM CaCl$_2$ and 1 mM MgSO$_4$ for 30 min. Cells were then washed twice with calcium free HBSS containing 1 mM MgSO$_4$ and subjected to analysis to measure calcium fluxes using Till Photonics digital microscope (Thermo Fisher Scientific, NJ, USA). Relative fluorescence ratio at wavelengths of 340 nM and 380 nM (F340/F380) was calculated for the assessment of cytoplasmic calcium levels.

2.10. Western blotting

BMMs cultured in 6-well tissue culture plates were treated with 100 ng/ml LPS or 50 ng/ml IL-4 for the indicated time points. For total cell lysates, BMMs or CD11b$^+$ cells isolated from livers were lysed in RIPA buffer (20 mM Tris-HCl; pH 7.5, 150 mM NaCl, 1 mM EDTA, 1 mM EGTA, 1% Nonidet P-40, 1% sodium deoxycholate) supplemented with a protease/phosphatase inhibitor cocktail (Pierce). Protein concentration was determined by bicinchoninic acid protein assay (BioRad), samples were resolved by SDS-page and subjected to western blot analysis. In some circumstances, myeloid cells isolated from liver with MACS columns were immediately lysed and subjected to western

blotting as described above.

For immunoblotting phospho-STAT1 (7649, Cell Signaling Technology), STAT1 (9172, Cell Signaling Technology), phospho-STAT3 (9145, Cell Signaling Technology), STAT3 (4904, Cell Signaling Technology), phospho-STAT6 (9361, Cell Signaling Technology), STAT6 (5397, Cell Signaling Technology), Plcγ2 (3872, Cell Signaling Technology), phospho-Plcγ2 (3871, Cell Signaling Technology) and β-Actin (A5441, Sigma) antibodies were used. When phosphorylated proteins are detected, westerns were stripped and re-blotted for the total non-phosphorylated protein.

2.11. Plaque assay for viral titration

LCMV plaque assay was performed by plating Vero cells in 6-well tissue culture plates at a density of 2×10^5 cell/ml and incubated overnight at 37 °C. Vero cells were then incubated with serially diluted liver lysates for 1 h at 37 °C. The viral inoculum was aspirated and cells were overlaid with 1:1 mixture of 2% low melting point agarose and $2\times$ medium containing 10% FBS. The plates were then incubated at 37 °C for 4 days. Post-infection the cells were fixed with 10% formaldehyde at room temperature for 2 h and finally stained with crystal violet. Plaques were counted and PFU was determined per gram of tissue.

2.12. In vitro restimulation assay

After obtaining a single cell suspension of spleen, splenocytes were resuspended at a density of 1×10^7 cells per ml and incubated with or without LCMV gp 61–80 peptide (1 ng/ml; AnaSpec) for 5 h in the presence of BD GolgiPlug (BD Biosciences). The cells were then surface stained followed by intracellular staining with IFNγ using BD Cytofix/Cytoperm Plus kit following manufacturer's protocol.

2.13. Statistics

Data is reported as mean and SD. Two sets of data were analyzed using two-tailed Student's *t*-test. Experiments with multiple comparisons were analyzed by a one-way or two-way analysis of covariance in conjunction with a Bonferroni post-hoc test. For survival studies the significance was determined by log-rank test. P value of < 0.05 is set as statistically significant, *p < 0.05 **p < 0.01, ***p < 0.001.

3. Results

3.1. Administration of clodronate-liposomes and anti-CSF1 antibody improves the survival of Prf−/− mice infected with LCMV

To evaluate the role of monocytes and macrophages in driving CSS progression, we used a well established CSS mouse model consisting of *Prf*$-/-$ animals, which have defective T cell cytotoxicity, infected with LCMV [11]. *Prf*$-/-$ mice also received control- or clodronate-liposomes two days prior to LCMV infection, on the day of infection (day 0), and 2 days post-infection (Fig. 1A). Depletion of circulating monocytes was confirmed by FACS 24 h after the last clodronate-liposome injection (Supplemental Fig. 1A). 100% of LCMV-infected *Prf*$-/$$-$ mice receiving control-liposomes died within 20 days, as previously described [11]. Animals treated with clodronate-liposomes had significantly improved survival (Fig. 1B) and showed reduced viral burden in the liver measured 8 days post-infection (Fig. 1C). While control-liposome treated mice showed a significant upregulation of circulating pro-inflammatory cytokines and chemokines measured 3 and 8 days post-infection compared to non-infected PBS controls (Fig. 1D and E; light bars), administration of clodronate-liposomes significantly blunted TNFα, IFNγ, CCL3, CCL4 and CCL5 induction (Fig. 1D and E; dark bars). By contrast, the levels of the anti-inflammatory cytokine IL-10 were notably elevated in the clodronate-liposome group (Fig. 1D). In
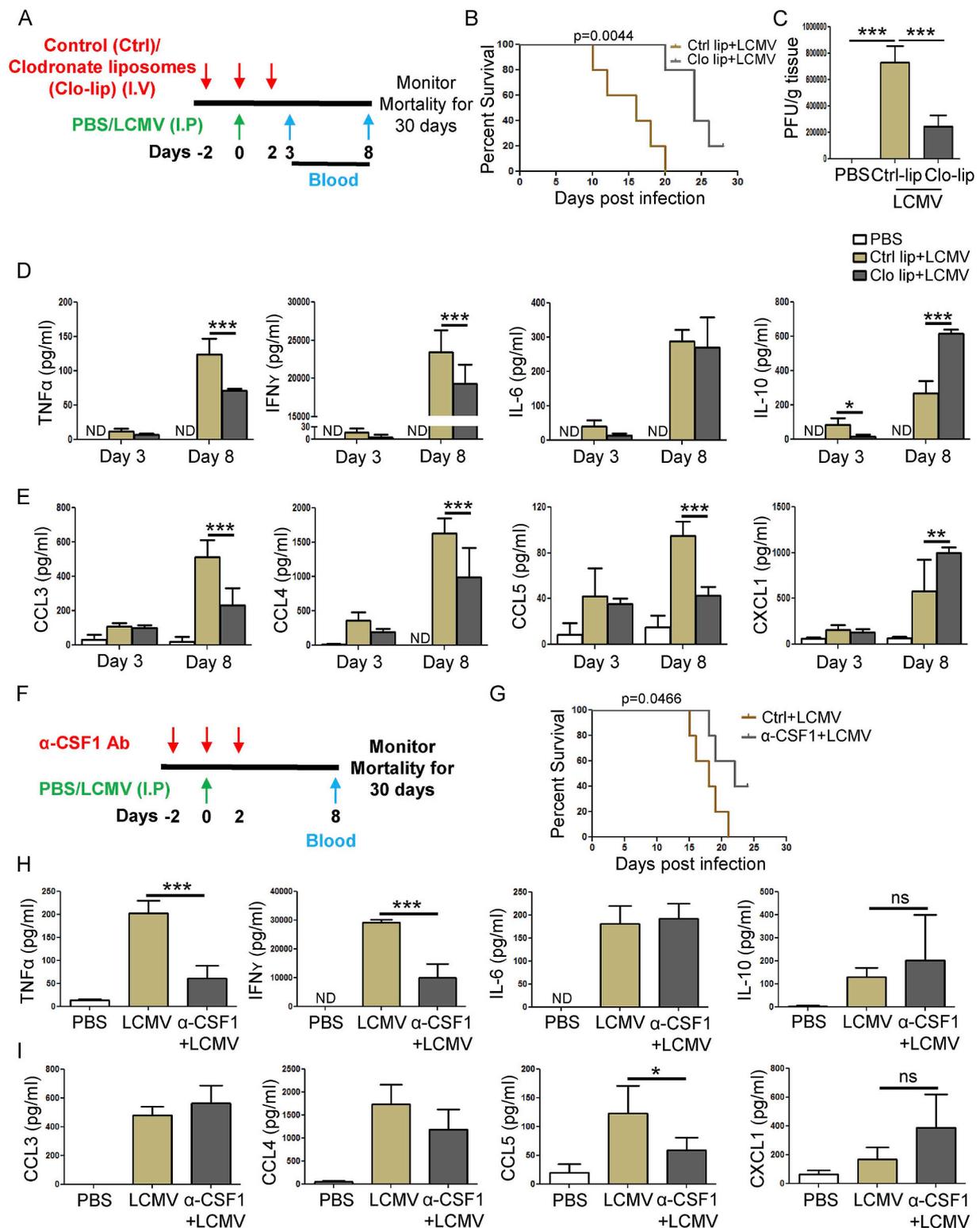
Fig. 1. Clodronate-liposome and anti-CSF1 antibody improve the survival of LCMV-infected *Prf−/−* mice. **(A)** Schematic representation of LCMV-induced CSS and clodronate-liposome treatment in *Prf−/−* mice. *Prf−/−* mice were given 100 μl of clodronate-liposomes (Clo-lip) or control-liposomes (Ctrl-lip) on days −2, 0 and 2 (red arrows). On day 0 the mice were infected with 2 × 10⁵ PFU LCMV-Armstrong (green arrow). Blood was collected 3 and 8 days after infection for analysis (blue arrows). **(B)** Kaplan-Meier survival curves of LCMV-infected *Prf−/−* mice (n = 5 per group) treated with Ctrl-lip or Clo-lip. Log-rank test was used to determine the statistical significance. **(C)** Viral titer was determined in liver samples from mice in B. **(D–E)** Serum levels of indicated inflammatory cytokines **(D)** and chemokines **(E)** were assayed by Milliplex on days 3 and 8 post-infection. **(F)** Schematic representation of LCMV-induced CSS and anti-CSF1 antibody treatment in *Prf−/−* mice. **(G)** Kaplan-Meier survival curves of LCMV-infected *Prf−/−* mice (n = 5 per group) treated with or without α-CSF1 antibody. Log-rank test was used to determine the statistical significance. **(H–I)** Serum levels of indicated inflammatory cytokines **(H)** and chemokines **(I)** were assayed by Milliplex on days 8 post-infection. Data in **C, D, E, H** and **I** are the averages of 4–5 individual mice (mean and SD) and statistical significance was determined by two-way ANOVA. **p < 0.01, ***p < 0.001.

order to determine whether treatment with clodronate-liposomes improves the survival of LCMV-infected *Prf −/−* mice by reducing the number of activated CD8$^+$ T cells due to off target effects of the drug on dendritic cells, we examined the percentage and the activation status of CD8$^+$ T cells in the spleen of mice treated as in Fig. 1A and incubated ex-vivo with the LCMV peptide GP 61–80 for 5 h. As reported in earlier studies, we observed a significant increase in the percentage of CD8$^+$ T cells on day 8 post LCMV infection (Supplemental Fig. 1B). We also observed activation of CD8$^+$ T cells as determined by the surface expression of CD44 and staining for intracellular IFNγ (Supplemental Fig. 1C and D). Interestingly, the increase in CD8$^+$ T cells or their activation status was not different between control and clodronate-liposome groups (Supplemental Fig. 1B-D), suggesting that clodronate treatment does not impact CD8$^+$ T cell responses.

As an alternative approach for monocyte/macrophage depletion, we intraperitoneally injected *Prf −/−* mice with the CSF1 neutralizing antibody, a critical factor required for the survival and proliferation of monocytes and macrophages (Fig. 1F). Administration of anti-CSF1 antibody significantly improved the survival of LCMV-infected *Prf −/−* mice compared to IgG controls (Fig. 1G). The levels of serum cytokines and chemokines were also significantly reduced in animals receiving anti-CSF1 (Fig. 1H and I). Together, these findings indicate that early depletion of monocytes/macrophages prior to CSS development improves survival and significantly reduces the circulating levels of inflammatory cytokines and chemokines.

3.2. Clodronate-liposome treatment reduces inflammatory cytokine levels in mice with CpG-induced CSS

Next, we employed a non-genetic CSS model that involves repeated injections of the TLR9 agonist CpG (50 μg), administered every other day for 8 days, followed by sacrifice 24 h after the last injection (scheme in Fig. 2A). Monocytes/macrophages were depleted by 3 intravenous injections of clodronate-liposomes at 48 h intervals, beginning 2 days prior to starting CpG. Mice sacrificed 1 day after the last clodronate injection showed significant reduction of macrophages in spleen and liver, but not of neutrophils and dendritic cells (Supplemental Fig. 2A and B).

Clodronate-liposome treatment led to a milder form of CSS. White blood cell numbers (WBC) and platelet counts were improved (Fig. 2B and C) and splenomegaly and hepatomegaly were also partially prevented by clodronate-liposome treatment (Fig. 2D–F). While administration of clodronate-liposomes did not rescue the disrupted splenic architecture (Supplemental Fig. 2C), H&E staining of liver sections showed reduced inflammatory infiltrates, both around the veins and in the parenchyma (Fig. 2G white dotted line), and decreased number of veins obstructed with microthrombi (Fig. 2G black arrow; quantified in Fig. 2H and I) compared to control-liposomes. The percentages of liver F4/80$^+$CD11b$^+$ macrophages and Ly6C$^+$/CD11b$^+$ monocytes increased in mice injected with the TLR9 ligand compared to PBS controls (Fig. 2J and K and Supplemental Fig. 2D and E), but their numbers were only slightly reduced in the clodronate-liposome group, suggesting that depleting monocytes/macrophages during the initial stages of CSS development was not sufficient to ablate this population for the entire length of the experiment (Fig. 2J and K). Nevertheless, TNFα, IL-6 and IFNγ levels in the serum were significantly reduced in the clodronate-liposome group both 3 and 9 days after the first CpG injection (Fig. 2L and M). Furthermore, TNFα, IL-6 and IL-1β mRNA levels in the liver isolated on day 9 were also significantly reduced by clodronate-liposome administration (Fig. 2N). All together, these data suggest that monocyte/macrophage depletion by clodronate-liposomes before disease onset limits the induction of an overwhelming cytokine storm.

3.3. Loss of Plcγ2 in myeloid cells protects from the development of CSS

To further characterize the involvement of monocytes/macrophages

during CSS progression, we turned to animal models with aberrant macrophage responses. We previously demonstrated that *Plcγ2,* an enzyme activated downstream of TLRs, receptor tyrosine kinases, and integrins and a modulator of calcium levels, is activated in myeloid populations and controls the development of inflammation in murine models of arthritis [28,29]. We first confirmed Plcγ2 phosphorylation in CD11b$^+$ cells isolated from livers of mice with CpG-induced CSS (Supplemental Fig. 3A). Next, to examine whether loss of *Plcγ2* in myeloid populations protects from CSS, we crossed *Plcγ2* floxed mice with animals expressing Cre under the control of the Lysosome M promoter, herein referred to as *Plcγ2cKO* mice. We found that *Plcγ2cKO* mice developed milder CSS symptoms than WT and LysMCre animals, both used as controls. *Plcγ2cKO* mice displayed improved platelet numbers (Fig. 3A), although WBC counts were similar to control mice (Fig. 3B). The spleen and liver weights were partially but significantly reduced in *Plcγ2cKO* mice with CSS (Fig. 3C–E). Histological analysis revealed no damage of the splenic architecture (Supplemental Fig. 3B and C) and reduced inflammatory infiltrates and microthrombi in the liver (Fig. 3F–H). Serum IL-6 levels and IL-1β, IL-6 and TNFα transcripts in the liver were drastically reduced in *Plcγ2cKO* versus controls (Fig. 3I and J; CpG groups). Importantly, all these differences were not due to different basal inflammatory cytokine levels between the two genotypes (Fig. 3I and J; PBS groups). To determine the myeloid populations impacted by the loss of *Plcγ2*, we next performed FACS analysis in livers of mice with or without CSS. While the numbers of neutrophils were unchanged (Supplemental Fig. 3D), we observed a slight reduction in the percent of macrophages and monocytes in the *Plcγ2cKO* mice compared to controls (Fig. 3K and not shown). However, *ex-vivo* stimulation of *Plcγ2cKO* BMMs with 1 μM CpG for 24 h showed decreased production of IL-6 and TNFα compared to WT cells (Fig. 3L). These data indicate that Plcγ2 is critical for monocyte and macrophage responses during CSS progression and that its loss reduces inflammatory cytokine production, thereby ameliorating CSS clinical pathologies features.

3.4. Loss of Tmem178 accentuates inflammatory cytokine production in CpG-induced CSS

We recently reported that Tmem178 is a Plcγ2-dependent gene and a negative regulator of osteoclastogenesis [26]. RT-PCR analysis confirmed that Tmem178 levels are barely detectable in *Plcγ2 −/−* BMMs following adhesion to pRGD (Supplemental Fig. 4A). Furthermore, Immgen expression dataset revealed that Tmem178 expression is higher in macrophages and monocytes than neutrophils and dendritic cells, and no expression is found in T cells (Supplemental Fig. 4B). We confirmed these data by RT-PCR and show that Tmem178 elevels in CD3$^+$ T cells are negligible compared to macrophages (Supplemental Fig. 4C). To assess whether Tmem178 modulates inflammatory responses in the macrophages, WT and *Tmem178 −/−* BMMs were stimulated *in vitro* with CpG (1 μM). *Tmem178 −/−* BMMs produced significantly higher protein levels of IL-6 and TNFα (Fig. 4A). By contrast, IL-10 transcripts, an anti-inflammatory cytokine, were reduced in the *Tmem178* null cells (Supplemental Fig. 4D). Strikingly, *Tmem178 −/−* mice developed a more severe CpG-induced CSS phenotype than WT mice. We observed a significant increase in spleen size compared to WT (Fig. 4B and C). Although the liver weight was similar between the two cohorts (Fig. 4D), H&E-stained liver sections showed larger areas of inflammatory infiltrates and higher numbers of occluded veins in *Tmem178 −/−* mice (Fig. 4E–G). Platelet numbers were also decreased compared to WT animals, but WBC counts were similar between the two genotypes (Supplemental Fig. 4E and F). Supporting the hypothesis that Tmem178 is a negative regulator of monocyte/macrophage activation, *Tmem178 −/−* mice showed higher IL-6 levels in circulation (Fig. 4H) and increased IL-1β, IL-6 and TNFα transcripts in liver extracts compared to WT mice (Fig. 4I). FACS analysis revealed only a slight increase in the percent of F4/80$^+$CD11b$^+$ liver macrophages with no changes in neutrophil counts (Fig. 4J and Supplemental

Fig. 2. Clodronate-liposome treatment reduces inflammatory cytokine levels in mice with CpG-induced CSS. **(A)** Schematic representation of CpG-induced CSS and clodronate-liposome treatment. C57Bl/6 WT mice were injected with either PBS or CpG every other day as indicated by the green arrows. Starting 2 days prior to the first CpG injection the animals were given either 100 μl of control-liposomes or clodronate-liposomes as indicated by red arrows. **(B–C)** Blood was drawn on day 9 and sampled for WBC **(B)** and platelets **(C)**. **(D–E)** Representative spleen images are shown **(D)** and spleen weight was determined by measuring the ratio of spleen weight to body weight multiplied by 100 **(E)**. **(F)** Liver weight was determined by measuring the ratio of liver weight to body weight x 100. **(G–I)** H&E stained liver sections from mice injected with PBS as control or with CpG and either treated with Ctrl-lip or Clo-lip. Presence of hepatic inflammation (dotted white lines) and formation of microthrombi (black arrow) in **(G)** were quantified in **(H)** and **(I)**, respectively. The inflammatory score was determined by assessing the presence of inflammatory infiltrates around the veins and within the parenchyma and scored on a scale from 0, being the lowest, to 4, the highest **(H)**. Presence of microthrombi was quantified by calculating the percentage of veins occluded **(I)**. **(J)** The percentage of CD45^{+}Ly6G^{−}CD11b^{+}F4/80^{+} macrophages was determined in livers by FACS. **(K)** The percentage of CD45^{+}Ly6G^{−}CD11b^{+}Ly6C^{+} monocytes was determined in livers by FACS. **(L)** Serum levels of TNFα, IL-6 and IFNγ were assayed by Milliplex on day 3. **(M)** Serum levels of IL-6 were evaluated by ELISA on day 9. **(N)** mRNA expression of TNFα, IL-6 and IL-1β was assessed in the livers of mice treated as in **A** and sacrificed on day 9. Individual symbols in Figures **B**, **C**, **E** and **F** represent 1 mouse with horizontal lines representing the mean values. Bars in Figures **H-M** (n = 4 to 10 mice/group) represent mean and SD. Statistical significance was determined by two-tailed Student's *t*-test or one-way ANOVA for multiple comparisons. *p < 0.05, **p < 0.01, ***p < 0.001.
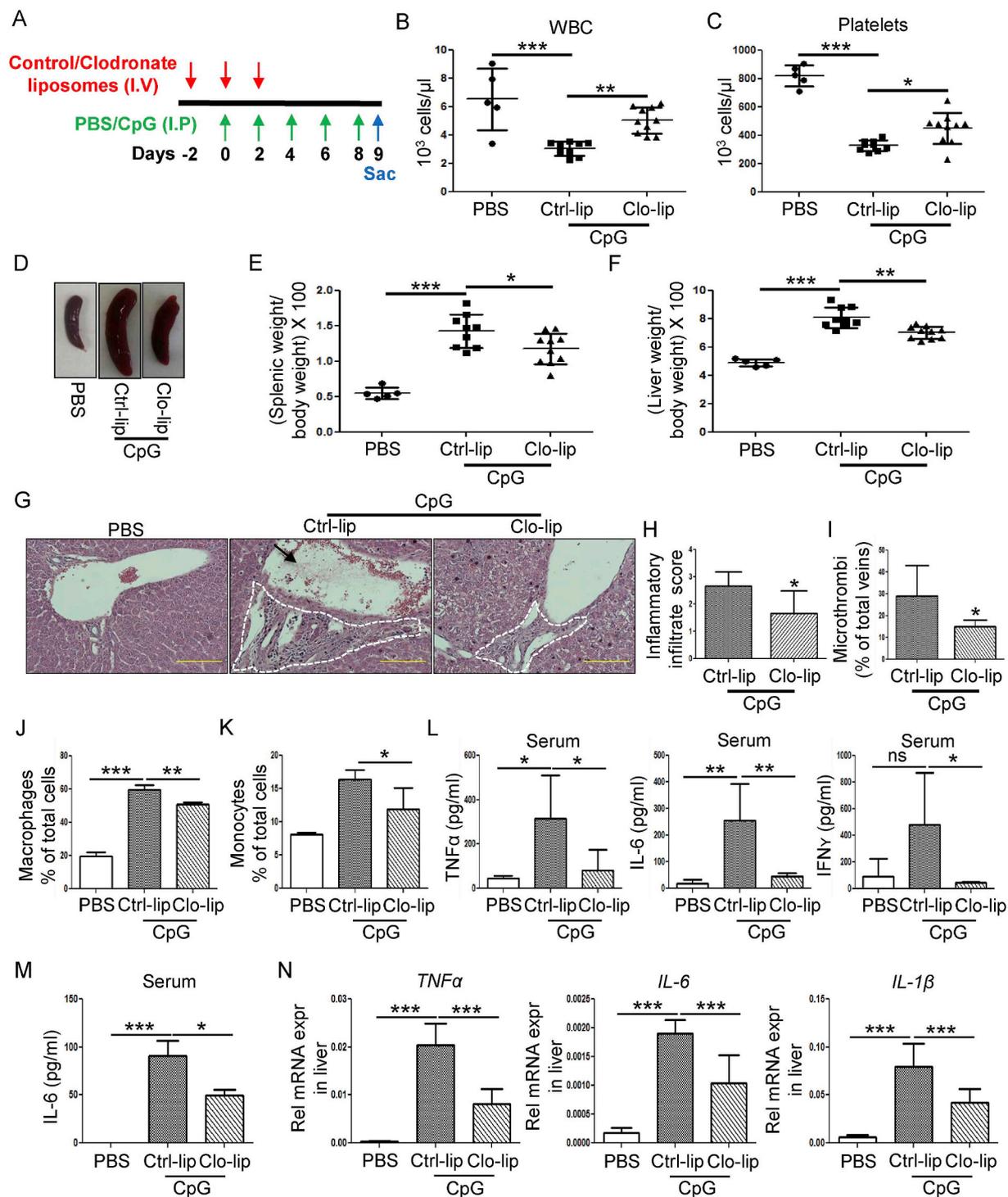
Fig. 4G), suggesting that loss of Tmem178 mainly affects monocyte/macrophage functionality rather than their numbers. Further supporting this hypothesis, F4/80$^+$ cells sorted with magnetic beads from the liver of *Tmem178−/−* mice injected with CpG expressed significantly more pro-inflammatory cytokines than their WT counterparts (Fig. 4K). These data suggest that loss of *Tmem178* worsens CSS development possibly by activating the monocytes and macrophages to produce more inflammatory cytokines.
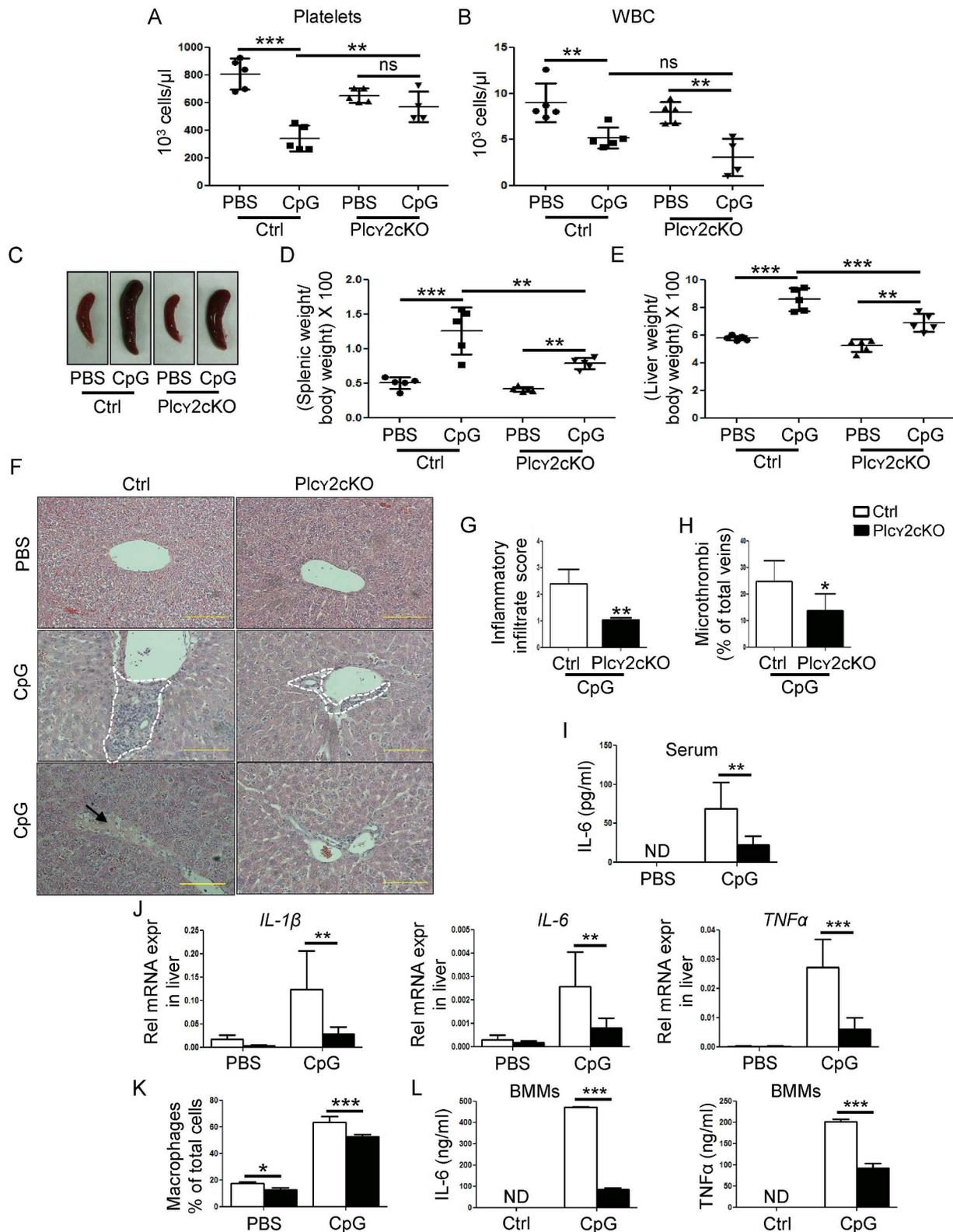
(caption on next page)

Fig. 3. Loss of *Plcγ2* in myeloid cells protects from the development of CSS. **(A–B)** The total platelet **(A)** and WBC **(B)** counts were analyzed in the blood on day 9 obtained from Ctrl and *Plcγ2cKO* mice treated with either PBS or CpG every other day for 8 days. **(C)** Representative spleens from Ctrl and *Plcγ2cKO* mice from indicated groups on day 9. **(D)** The splenic weight was determined by calculating the ratio of spleen weight versus total body weight x 100. **(E)** Liver weight was determined by calculating the ratio of liver weight versus body weight x 100. **(F–H)** H&E stained liver sections from indicated mice sacrificed 9 days after the initial CpG injection were scored for presence of hepatic inflammation (dotted white lines) and formation of microthrombi (black arrow) **(F)**. The inflammatory score was determined by assessing the presence of inflammatory infiltrates around the veins and within the parenchyma and scored on a scale from 0, being the lowest, to 4, the highest **(G)**. Presence of microthrombi was quantified by calculating the percentage of veins occluded **(H)**. **(I)** IL-6 levels in the serum were determined by ELISA on day 9. **(J)** The transcript levels of IL-1β, IL-6 and TNFα were assessed in liver extracts from Ctrl or *Plcγ2cKO* sacrificed on day 9. **(K)** The percentage of CD45$^+$Ly6G$^-$CD11b$^+$F4/80$^+$ macrophages in liver was determined by FACS on day 9. **(L)** Secretion of IL-6 and TNFα in supernatants of Ctrl or *Plcγ2cKO* BMMs stimulated with CpG for 24 h was measured by ELISA. Individual symbols in FiguresA, B, D and E represent 1 mouse with horizontal lines representing the mean values. Bars in Figures **G-L** (n = 4–5 mice/group) represent mean and SD. Statistical significance was determined by two-tailed Student's *t*-test or two-way ANOVA for multiple comparisons. *p < 0.05, **p < 0.01, ***p < 0.001.

3.5. Loss of Tmem178 leads to early mortality following LCMV-induced CSS

To further evaluate the role of Tmem178 in LCMV-induced CSS, we generated mice that lack perforin and Tmem178 (*Prf-Tmem178* double knockout*)*, infected with LCMV (Fig. 5A) and observed that these animals succumbed earlier than *Prf−/−* animals following the infection (Fig. 5B). Analysis of the serum cytokines on days 3 and 8 post-infection revealed significantly increased levels of IL-6 in the *Prf-Tmem178* double knockout mice (Fig. 5C). Surprisingly, we did not observe any difference in TNFα, IFNγ and IL-10 levels between the two groups (Fig. 5C), although it is possible that their levels have already reached a plateau. Furthermore, we observed an increase in CCL3 and a trend for increased CCL4, CCL5 and CXCL1 chemokines in LCMV-infected *Prf-Tmem178* double knockout compared to *Prf−/−* mice (Fig. 5D). All together the results from the TLR9 and LCMV-induced CSS mouse models indicate that Tmem178 is a negative regulator of inflammatory cytokines in the monocytes/macrophages acting in a negative feed-back loop axis downstream of Plcγ2 in attempt to limit the overwhelming cytokine storm during CSS progression.

3.6. Tmem178 deficiency drives a pro-inflammatory macrophage phenotype

To further address the role of Tmem178 on macrophage activation, we stimulated WT and *Tmem178−/−* BMMs *in vitro* with 100 ng/ml of LPS. mRNA and protein levels of IL-6, TNFα and IL-1β were increased in *Tmem178−/−* cells compared to WT (Fig. 6A and B). We also observed a significant increase in the macrophage markers associated with a pro-inflammatory or M1-like phenotype iNOS, CCL5 and IRF5, and higher production of NO in the *Tmem178* null cultures (Fig. 6C and D). Phospo-(p) STAT1 and p-STAT3, signals activated in M1 polarized macrophages, were also increased in cell lysates from *Tmem178−/−* BMMs treated with LPS (Fig. 6E). Interestingly, IL-4 treatment, which induces M2 polarization, led to similar p-STAT6 and expression of Arginase 1 and PPARγ in both the genotypes (Supplemental Fig. 5A and B). We previously demonstrated that loss of Tmem178 activates calcium signaling in osteoclasts [26]. Similarly, *Tmem178*-deficient BMMs had increased basal intracellular calcium levels compared with WT (Fig. 6F). To confirm that calcium signaling is required for M1 macrophage responses, treatment with 10 μM BAPTA, an intracellular chelator of calcium, significantly reduced LPS-mediated increase of inflammatory cytokines in both WT and *Tmem178−/−* cells (Fig. 6G).

Next, we wondered whether Tmem178 levels are modulated in macrophages from mice with CSS. Thus, we FACS sorted CD11b$^+$F4/80$^+$ macrophages from livers of WT mice with TLR9-induced CSS and found a significant reduction in Tmem178 transcripts compared to healthy controls (Fig. 6H). Furthermore, exposure of macrophages to plasma obtained from 13 sJIA patients with active disease strongly reduced Tmem178 mRNA levels compared to serum from healthy controls (Fig. 6I). In sum, Tmem178 is a negative regulator of pro-inflammatory macrophages through regulation of calcium levels, and reduction of Tmem178 levels is observed after prolonged exposure to an inflammatory milieu.

4. Discussion

Despite the development of cytokine-targeted therapeutic approaches, mortality associated with CSS remains significant, in part due to delayed recognition and variability in the responses of the patients to the available treatments [1,6,10]. Because monocytes and macrophages are expanded in CSS and cytokines produced by these cells are paramount to its pathogenesis, we aimed to identify their contribution to CSS initiation and the signaling pathways that would drive their activation. By using established mouse models of CSS, which resemble the clinical manifestations of the disease in the patients, we demonstrate that depletion of monocytes and macrophages prior to CSS onset limits the development of full-blown disease, prolongs survival and reduces inflammatory cytokine levels. Our study uncovers a key role for Plcγ2 dependent signaling pathways in the pathogenesis of CSS. Our data also indicate that Plcγ2 can drive a negative feedback axis to restrain the overwhelming macrophage inflammatory response via induction of Tmem178, a negative regulator of calcium fluxes which modulates M1-like pro-inflammatory macrophage polarization.

Insights from examining genetic and environmental factors associated with CSS primarily implicate T cell cytotoxic defects and T cell hyperactivity following viral infections inducing elevated IFNγ levels and activating monocyte/macrophage responses [11]. However, a cluster of genes associated with innate immune responses is elevated in patients with sub-clinical and clinical CSS, regardless of the defects in T cell cytotoxicity. Buttressing the importance of monocytes/macrophages to CSS development, a *de novo* missense mutation in the NLRC4 inflammasome, a protein complex required for the production of active IL-1β and IL-18, was shown to lead to recurrent CSS episodes and increased inflammatory cytokine production in human monocytes [20]. Imbalance between IL-18 and its natural inhibitor IL-18BP was also shown to lead to severe CSS in response to TLR9 stimulation [30]. A recent unbiased single cell RNA-sequencing analysis performed in cancer models developing CSS after being treated with CAR-T cell therapy confirmed elevated expression of pro-inflammatory cytokines and chemokine by the monocytes [23]. Furthermore, in animal models, administration of engineered CAR-T cells expressing CD40 ligand resulted in more severe CSS due to the interaction with CD40 receptor expressed on the macrophages [24]. Ablation of monocytes/macrophages by clodronate-liposomes prevented the mortality [23,24]. Intriguingly, a mouse model of TLR9-induced CSS indicated that the expansion of monocytes and macrophages was due to extramedullary hematopoiesis occurring in the spleen and liver, thus rendering CCR2 blockade, as an approach to reduce recruitment of these inflammatory cells to peripheral organs, unsuccessful [21].

In this study, we find that administration of clodronate-liposomes or neutralization of CSF1 to deplete monocytes/macrophages prior to viral infection in *Prf−/−* mice prolongs survival and reduces the pro-inflammatory cytokine levels. By contrast IL-10 is increased, most likely due to suppression of IFNγ and/or polarization of the remaining macrophages toward an M2-like, anti-inflammatory phenotype [31]. Although this mouse model is known to be dependent on CD8$^+$ T cells, we confirmed that treatment with clodronate-liposomes did not alter the
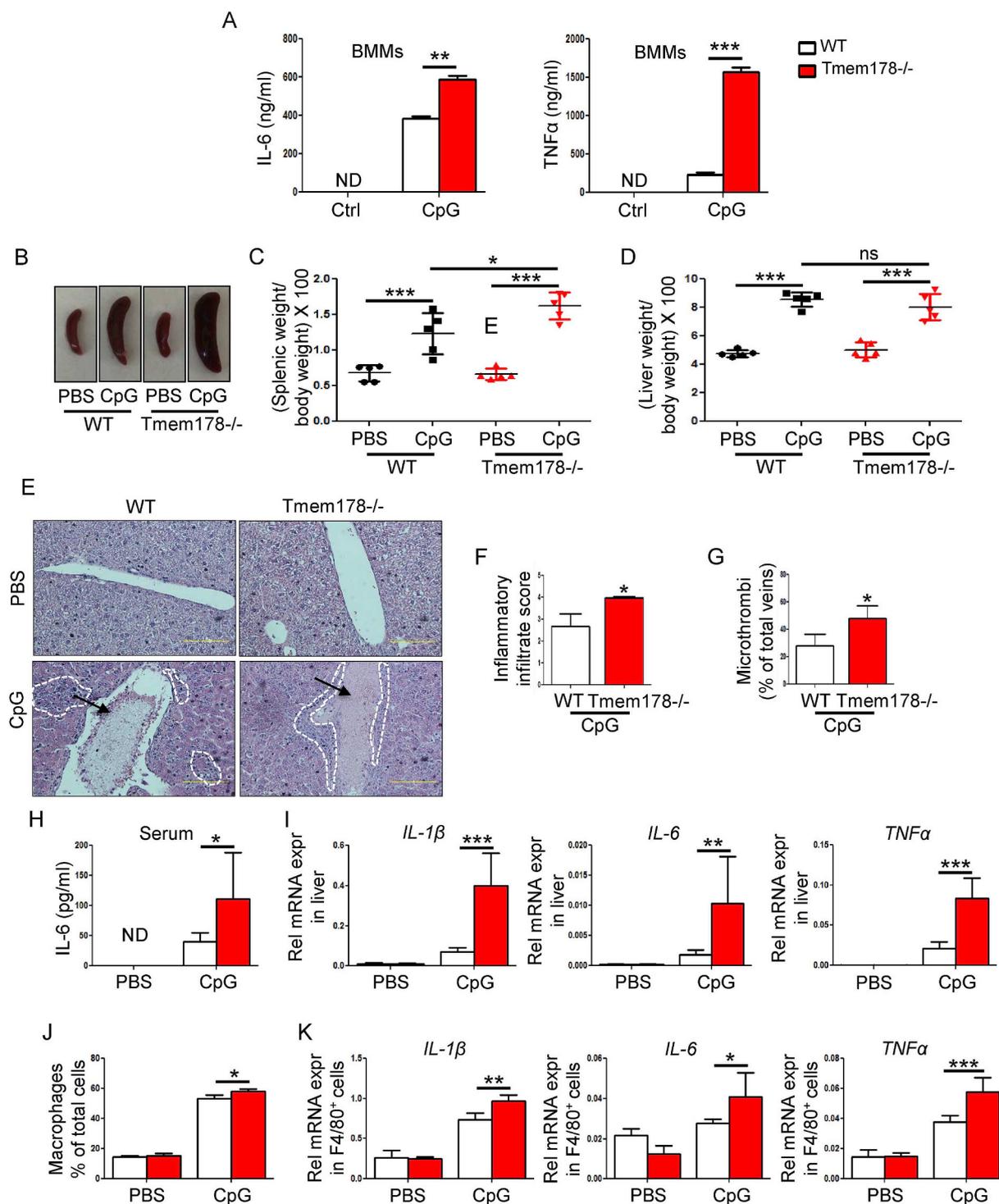
Fig. 4. Loss of *Tmem178* accentuates inflammatory cytokine production in CpG-induced CSS. **(A)** The levels of IL-6 and TNFα were measured by ELISA in the supernatant of WT and *Tmem178−/−* BMMs stimulated with 1 μM of CpG for 24 h. **(B–C)** Representative images of spleen size **(B)** and quantification of spleen weight **(C)** in WT and *Tmem178−/−* mice injected every other day with either PBS or CpG and sacrificed on day 9 for analysis. **(D)** The extent of hepatomegaly was quantified by measuring the ratio of liver weight to body weight x 100. **(E)** Representative H&E stained liver sections highlight the presence of inflammatory infiltrates (indicated by white dotted lines) and formation of microthrombi (black arrows). **(F)** The inflammatory score was determined by analyzing the extent of inflammatory infiltrates around the veins and the parenchyma with 0, the lowest, and 4, the highest score. **(G)** Presence of microthrombi was quantified by calculating the percentage of veins occluded. **(H)** Serum levels of IL-6 were evaluated by ELISA on day 9. **(I)** The transcript levels of inflammatory cytokines were measured in the liver of WT and *Tmem178* deficient mice on day 9. **(J)** Quantification of the % of CD45$^+$Ly6G$^-$CD11b$^+$F4/80$^+$ macrophages in the liver of WT and *Tmem178* deficient mice was assessed on day 9. **(K)** The transcript levels of IL-1β, IL-6 and TNFα were assessed in F4/80$^+$ cells sorted with magnetic beads from the livers of WT and *Tmem178* deficient mice on day 9 after CpG treatment. Individual symbols in Figures C and D represent 1 mouse with horizontal lines representing the mean values. Bars in Figures **A, F-K** (n = 5 mice/group) represent mean and SD. Statistical significance was determined by two-tailed Student's *t*-test or two-way ANOVA for multiple comparisons. *p < 0.05, **p < 0.01, ***p < 0.001.
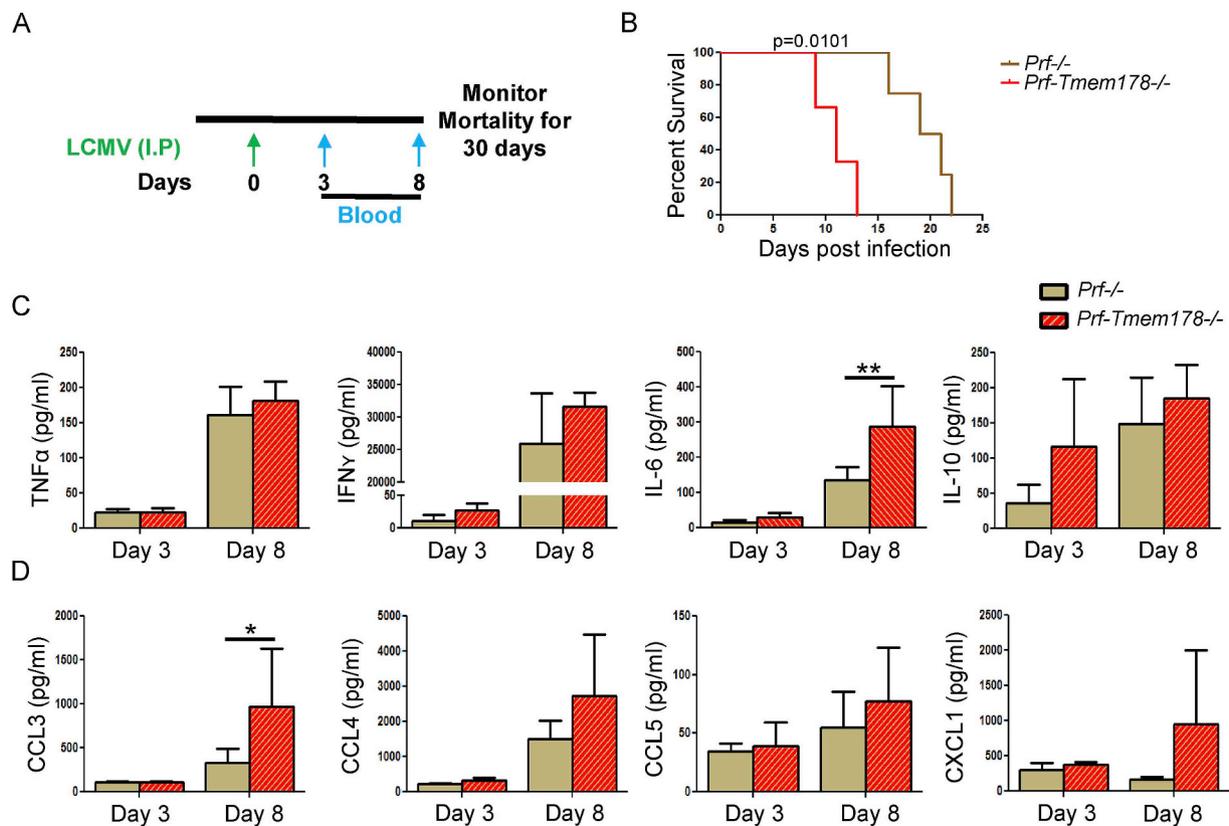
Fig. 5. Loss of Tmem178 leads to early mortality following LCMV-induced CSS. **(A)** Schematic representation of LCMV-induced CSS in *Prf−/−* and *Prf-Tmem178* double knockout mice. On day 0 both cohorts were infected with 2×10^5 PFU LCMV-Armstrong and blood was collected 3 and 8 days after infection for analysis. **(B)** Kaplan-Meier survival curves of LCMV-infected *Prf−/−* and *Prf-Tmem178* double knockout mice (n = 6–8 mice per group). Log-rank test was used to determine the statistical significance. **(C–D)** Serum levels of indicated inflammatory cytokines **(C)** and chemokines **(D)** were assayed by Milliplex on days 3 and 8 post LCMV-infection. Data in **C** and **D** are the averages of 4–5 individual mice (mean and SD) and statistical significance was determined by two-way ANOVA. *p < 0.05, **p < 0.01.

percent and activation status of CD8$^+$ T cells, thus indicating that the overwhelming cytokine storm cannot be perpetrated in the absence of monocytes/macrophages at disease onset. In a second CSS mouse model dependent on TLR9 activation we also find that administration of clo-dronate-liposomes 2 days prior, the day of, and 2 days after the first CpG injection is sufficient to ameliorate CSS features. Intriguingly, while dendritic cell and neutrophil numbers were unchanged, we observed only about 40% reduction of macrophages in spleen and liver of these mice 3 days after the first CpG injection, and their count was only reduced by 10% on day 9. Nevertheless, the levels of macrophage-produced inflammatory cytokines remained significantly decreased during disease progression. These results suggest that monocytes/macrophages play a critical role in disease initiation and in the maintenance of a prolonged inflammatory response. We cannot exclude that by day 9 the remaining macrophages acquire an M2-like, anti-inflammatory phenotype, which would explain the high levels of IL-10 and the reduced expression of pro-inflammatory cytokines.

Macrophages are highly versatile innate immune cells with the capacity to polarize to an M1-like pro-inflammatory or M2-like anti-inflammatory phenotype, depending upon the environmental milieu [32–35]. Monocytes from sJIA patients with active disease show mixed M1/M2 markers [15,36]. Similar findings are observed in CSS patients, with presence of macrophages producing high levels of pro-inflammatory cytokines, but also accumulation of hemophagocytes, differentiated macrophages that phagocytose other cells and express molecules conventionally involved in anti-inflammatory responses [10,19,37–40]. The signaling pathways driving monocyte/macrophage pro-inflammatory responses in CSS are not fully understood. Our data demonstrate that Plcγ2 is required for M1 macrophage responses to

drive CSS. There is considerable evidence that aberrant Plcγ2 signaling in immune cells is involved in auto-inflammatory and autoimmune diseases in humans and mice. Initial studies identified mutations in the human *PLCγ2* gene that dysregulate immune homeostasis leading to inflammatory disorders [41,42]. Mouse models carrying *Plcγ2* gain-of-function mutations develop spontaneous inflammation and auto-immunity [43]. Conversely, *Plcγ2*-deficient mice are protected from joint inflammation in models of arthritis due to reduced recruitment of neutrophils at the site of inflammation [29]. In the context of CSS, we do not find changes in neutrophil numbers either in WT or in the *Plcγ2cKO* mice, suggesting that other myeloid populations are responsible for mounting the overwhelming inflammatory responses. Although macrophage and monocyte numbers are only slightly decreased in tissues from *Plcγ2cKO* mice with CSS, the *ex vivo* analysis show a significant reduction in inflammatory cytokine levels produced by these cells. This result suggests that Plcγ2 drives monocyte and macrophage inflammatory responses.

Intriguingly, our study also suggests the existence of a negative feedback loop downstream of Plcγ2 via the induction of Tmem178, a negative regulator of calcium fluxes, specifically expressed in macrophages and monocytes, but not in T cells. Loss of *Tmem178* increases calcium levels in macrophages, supports M1 macrophage polarization and leads to a more severe CSS phenotype. The increase in disease severity in these animals is likely due to a combination of increased pro-inflammatory cytokines and reduced IL-10 levels. Indeed, neutralization of IL-10 in WT animals was shown to lead to a fulminant TLR9-induced CSS phenotype [22]. Although *Tmem178−/−* animals do not die following TLR9 stimulation, they succumb faster in the LCMV-CSS model. These results reflect the fact that pro-inflammatory cytokines
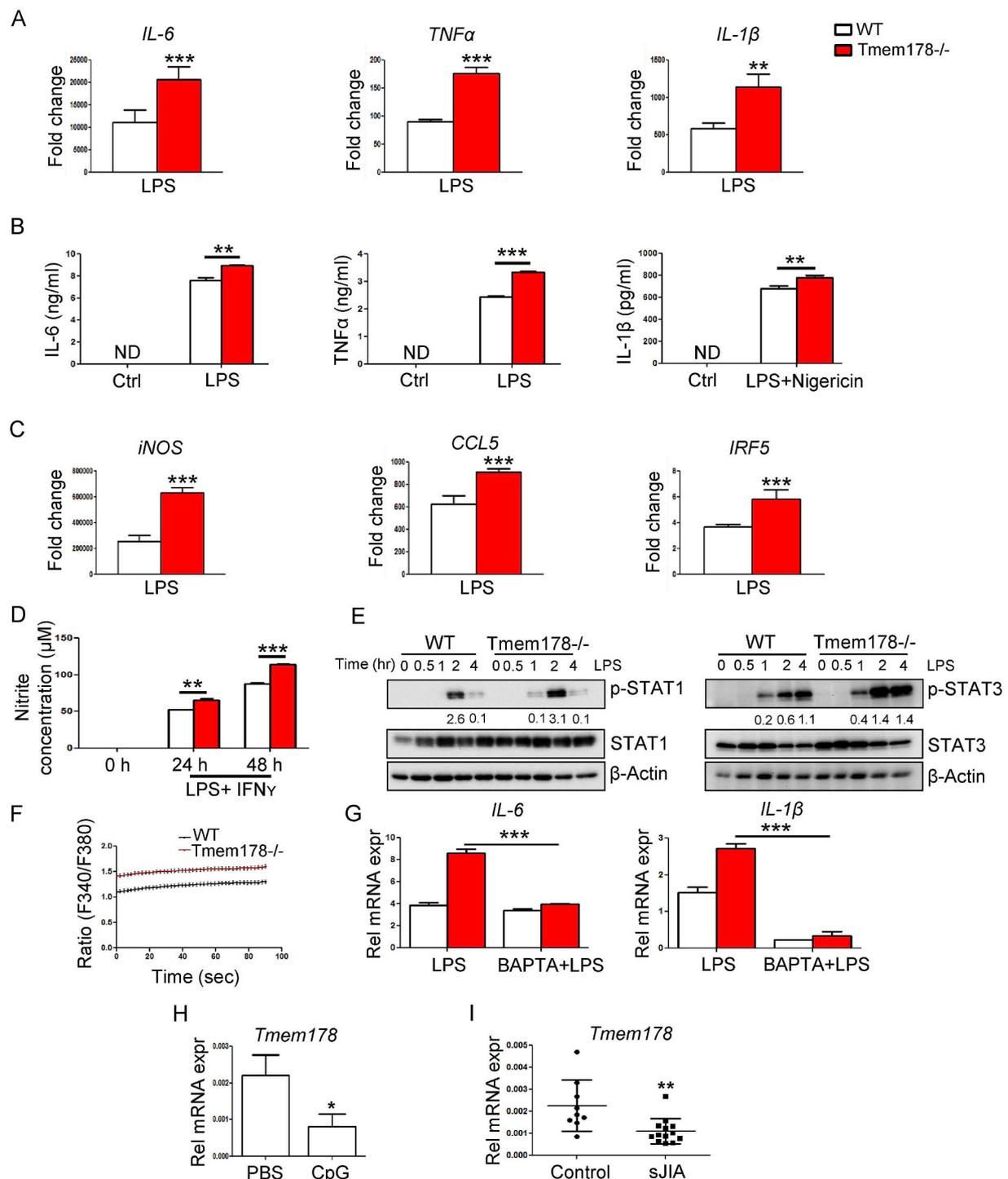
Fig. 6. Tmem178 deficiency drives a pro-inflammatory macrophage phenotype. **(A)** RT-qPCR analysis of IL-6, TNFα and IL-1β in BMMs derived from WT and *Tmem178 − / −* mice stimulated with 100 ng/ml of LPS for 4 h. Data are expressed as fold change in comparison to unstimulated WT BMMs. **(B)** IL-6 and TNFα were measured by ELISA in the supernatant of BMMs stimulated with 100 ng/ml of LPS for 24 h. IL-1β levels were assessed in BMMs treated with LPS (100 ng/ml) for 2 h followed by 7.5 μM nigericin for 15 min. **(C)** The transcript levels of iNOS, CCL5 and IRF5 were determined by RT-qPCR analysis in BMMs stimulated with 100 ng/ml of LPS for 4 h. Data are expressed as fold change versus unstimulated WT BMMs. **(D)** Nitrite concentration was measured in the supernatant of BMMs stimulated with LPS (100 ng/ml) and IFNγ (100 ng/ml) for 24 and 48 h by Griess assay. **(E)** BMMs were stimulated with LPS for indicated times and subjected to western blot analysis for phospho-STAT1, STAT1, phospho-STAT3 and STAT3. β-Actin was used as a loading control. Quantification was done by analyzing the ratio of the phospho-proteins to their respective total non-phospho protein form. **(F)** Intracellular calcium fluxes were measured in WT (black) and *Tmem178 − / −* (red) BMMs and incubated with 2 μM Fura-2-AM for 30 min prior to imaging. 82 WT cells and 74 *Tmem178 − / −* cells were analyzed and results were represented as mean and SEM. **(G)** BMMs were treated with 10 μM BAPTA 1 h prior to stimulation with 100 ng/ml of LPS and the transcript levels of IL-6 and IL-1β were determined by RT-qPCR. **(H)** Relative mRNA expression of Tmem178 was determined in CD11b⁺F4/80⁺ macrophages sorted from the liver of PBS or CpG-treated mice on day 9 (n = 3/ group). **(I)** The transcripts levels of Tmem178 were measured in macrophages treated with either healthy control (n = 9) or sJIA plasma (n = 13) for 4 h. Each symbol in Fig. **I** represents 1 individual sample with horizontal lines representing the mean values. The statistical significance was determined by two-way ANOVA. *p < 0.05, **p < 0.01, ***p < 0.001.

are major players in LCMV-induced CSS [13]. Perhaps, the most important aspect of our work is the observation that Tmem178 levels are downregulated in macrophages following exposure to plasma from sJIA with active disease and in macrophages from mice with CSS. While the mechanism leading to Tmerm178 downregulation remains to be determined, these results emphasize that loss of Tmem178 drives macrophage pro-inflammatory responses thus providing mechanistic insights for dysregulated innate immune activation in CSS.

5. Conclusion

Although the exact causes of CSS are not known, apart from viral infections in patients with mutations in cytotoxic pathways, recent evidence [23,24] and our data demonstrate that monocytes and macrophages are important drivers of CSS initiation and progression in both T cell-dependent and T cell-independent CSS models. In this study, we identified a novel Plcγ2/Tmem178 axis as a modulator of inflammatory cytokine production by monocytes/macrophages in CSS. This work provides the basis to evaluate the Plcγ2/Tmem178 axis in patients with sJIA to predict which subset of patients are more likely to develop CSS and underscore the potential role for monocyte/macrophage-based therapies for these patients.

Authors contribution

S. Mahajan and R. Faccio designed the experiments; S. Mahajan, C. Decker, Z. Yang performed the experiments; E. Mellins provided patient plasma samples, discussed the data and contributed to writing the paper; S. Mahajan, C. Decker, Z. Yang, D. Veis and R. Faccio analyzed and discussed the data; S. Mahajan and R. Faccio wrote the paper.

Conflicts of interest

The authors declare no conflict of interest.

Acknowledgments

Appendix A. Supplementary data

Supplementary data to this article can be found online at https://doi.org/10.1016/j.jaut.2019.02.005.

References

[1] S.W. Canna, E.M. Behrens, Making sense of the cytokine storm: a conceptual framework for understanding, diagnosing, and treating hemophagocytic syndromes, Pediatr. Clin. 59 (2012) 329–344.

[2] Q. Liu, Y.H. Zhou, Z.Q. Yang, The cytokine storm of severe influenza and development of immunomodulatory therapy, Cell. Mol. Immunol. 13 (2016) 3–10.

[3] J.I. Henter, G. Elinder, O. Soder, M. Hansson, B. Andersson, U. Andersson, Hypercytokinemia in familial hemophagocytic lymphohistiocytosis, Blood 78 (1991) 2918–2922.

[4] M. Feldmann, S.R. Maini, Role of cytokines in rheumatoid arthritis: an education in pathophysiology and therapeutics, Immunol. Rev. 223 (2008) 7–19.

[5] J.N. Kochenderfer, M.E. Dudley, S.A. Feldman, W.H. Wilson, D.E. Spaner, I. Maric, et al., B-cell depletion and remissions of malignancy along with cytokine-associated toxicity in a clinical trial of anti-CD19 chimeric-antigen-receptor-transduced T cells, Blood 119 (2012) 2709–2720.

[6] M.L. Davila, I. Riviere, X. Wang, S. Bartido, J. Park, K. Curran, et al., Efficacy and toxicity management of 19-28z CAR T cell therapy in B cell acute lymphoblastic leukemia, Sci. Transl. Med. 6 (2014) 224–225.

[7] A.A. Grom, M. Passo, Macrophage activation syndrome in systemic juvenile rheumatoid arthritis, J. Pediatr. 129 (1996) 630–632.

[8] S. Sawhney, P. Woo, K.J. Murray, Macrophage activation syndrome: a potentially fatal complication of rheumatic disorders, Arch. Dis. Child. 85 (2001) 421–426.

[9] G.S. Schulert, A.A. Grom, Macrophage activation syndrome and cytokine-directed therapies, Best Pract. Res. Clin. Rheumatol. 28 (2014) 277–292.

[10] A.A. Grom, A. Horne, F. De Benedetti, Macrophage activation syndrome in the era of biologic therapy, Nat. Rev. Rheumatol. 12 (2016) 259–268.

[11] M.B. Jordan, D. Hildeman, J. Kappler, P. Marrack, An animal model of hemophagocytic lymphohistiocytosis (HLH): CD8+ T cells and interferon gamma are essential for the disorder, Blood 104 (2004) 735–743.

[12] G.E. Janka, Familial and acquired hemophagocytic lymphohistiocytosis, Annu. Rev. Med. 63 (2012) 233–246.

[13] R. Das, P. Guan, L. Sprague, K. Verbist, P. Tedrick, Q.A. An, et al., Janus kinase inhibition lessens inflammation and ameliorates disease in murine models of hemophagocytic lymphohistiocytosis, Blood 127 (2016) 1666–1675.

[14] C.E. Terrell, M.B. Jordan, Perforin deficiency impairs a critical immunoregulatory loop involving murine CD8(+) T cells and dendritic cells, Blood 121 (2013) 5184–5191.

[15] N. Fall, M. Barnes, S. Thornton, L. Luyrink, J. Olson, N.T. Ilowite, et al., Gene expression profiling of peripheral blood from patients with untreated new-onset systemic juvenile idiopathic arthritis reveals molecular heterogeneity that may predict macrophage activation syndrome, Arthritis Rheum. 56 (2007) 3793–3804.

[16] M. Yanagimachi, T. Naruto, T. Miyamae, T. Hara, M. Kikuchi, R. Hara, et al., Association of IRF5 polymorphisms with susceptibility to macrophage activation syndrome in patients with juvenile idiopathic arthritis, J. Rheumatol. 38 (2011) 769–774.

[17] T. Krausgruber, K. Blazek, T. Smallie, S. Alzabin, H. Lockstone, N. Sahgal, et al., IRF5 promotes inflammatory macrophage polarization and TH1-TH17 responses, Nat. Immunol. 12 (2011) 231–238.

[18] E.E. Zoller, J.E. Lykens, C.E. Terrell, J. Aliberti, A.H. Filipovich, P.M. Henson, et al., Hemophagocytosis causes a consumptive anemia of inflammation, J. Exp. Med. 208 (2011) 1203–1214.

[19] A.D. Billiau, T. Roskams, R. Van Damme-Lombaerts, P. Matthys, C. Wouters, Macrophage activation syndrome: characteristic findings on liver biopsy illustrating the key role of activated, IFN-gamma-producing lymphocytes and IL-6- and TNF-alpha-producing macrophages, Blood 105 (2005) 1648–1651.

[20] S.W. Canna, A.A. de Jesus, S. Gouni, S.R. Brooks, B. Marrero, Y. Liu, et al., An activating NLRC4 inflammasome mutation causes autoinflammation with recurrent macrophage activation syndrome, Nat. Genet. 46 (2014) 1140–1146.

[21] L.K. Weaver, N. Chu, E.M. Behrens, TLR9-mediated inflammation drives a Ccr2-independent peripheral monocytosis through enhanced extramedullary monocytopoiesis, Proc. Natl. Acad. Sci. U. S. A. 113 (2016) 10944–10949.

[22] E.M. Behrens, S.W. Canna, K. Slade, S. Rao, P.A. Kreiger, M. Paessler, et al., Repeated TLR9 stimulation results in macrophage activation syndrome-like disease in mice, J. Clin. Invest. 121 (2011) 2264–2277.

[23] M. Norelli, B. Camisa, G. Barbiera, L. Falcone, A. Purevdorj, M. Genua, et al., Monocyte-derived IL-1 and IL-6 are differentially required for cytokine-release syndrome and neurotoxicity due to CAR T cells, Nat. Med. 24 (2018) 739–748.

[24] T. Giavridis, S.J.C. van der Stegen, J. Eyquem, M. Hamieh, A. Piersigilli, M. Sadelain, CAR T cell-induced cytokine release syndrome is mediated by macrophages and abated by IL-1 blockade, Nat. Med. 24 (2018) 731–738.

[25] V. Piccolo, A. Curina, M. Genua, S. Ghisletti, M. Simonatto, A. Sabo, et al., Opposing macrophage polarization programs show extensive epigenomic and transcriptional cross-talk, Nat. Immunol. 18 (2017) 530–540.

[26] C.E. Decker, Z. Yang, R. Rimer, K.H. Park-Min, C. Macaubas, E.D. Mellins, et al., Tmem178 acts in a novel negative feedback loop targeting NFATc1 to regulate bone mass, Proc. Natl. Acad. Sci. U. S. A. 112 (2015) 15654–15659.

[27] A. Hashimoto, K. Takeda, M. Inaba, M. Sekimata, T. Kaisho, S. Ikehara, et al., Cutting edge: essential role of phospholipase C-gamma 2 in B cell development and function, J. Immunol. 165 (2000) 1738–1742.

[28] V. Cremasco, E. Benasciutti, M. Cella, M. Kisseleva, M. Croke, R. Faccio, Phospholipase C gamma 2 is critical for development of a murine model of inflammatory arthritis by affecting actin dynamics in dendritic cells, PLoS One 5 (2010) e8909.

[29] V. Cremasco, D.B. Graham, D.V. Novack, W. Swat, R. Faccio, Vav/Phospholipase Cgamma2-mediated control of a neutrophil-dependent murine model of rheumatoid arthritis, Arthritis Rheum. 58 (2008) 2712–2722.

[30] C. Girard-Guyonvarc'h, J. Palomo, P. Martin, E. Rodriguez, S. Troccaz, G. Palmer, et al., Unopposed IL-18 signaling leads to severe TLR9-induced macrophage activation syndrome in mice, Blood 131 (2018) 1430–1441.

[31] P. Chomarat, M.C. Rissoan, J. Banchereau, P. Miossec, Interferon gamma inhibits interleukin 10 production by monocytes, J. Exp. Med. 177 (1993) 523–527.

[32] P.J. Murray, J.E. Allen, S.K. Biswas, E.A. Fisher, D.W. Gilroy, S. Goerdt, et al., Macrophage activation and polarization: nomenclature and experimental guidelines, Immunity 41 (2014) 14–20.

[33] P.J. Murray, Macrophage polarization, Annu. Rev. Physiol. 79 (2017) 541–566.

[34] A. Sica, A. Mantovani, Macrophage plasticity and polarization: in vivo veritas, J. Clin. Invest. 122 (2012) 787–795.

[35] A. Mantovani, A. Sica, M. Locati, Macrophage polarization comes of age, Immunity 23 (2005) 344–346.

[36] C. Macaubas, K.D. Nguyen, A. Peck, J. Buckingham, C. Deshpande, E. Wong, et al., Alternative activation in systemic juvenile idiopathic arthritis monocytes, Clin. Immunol. 142 (2012) 362–372.

[37] E.M. Behrens, G.A. Koretzky, Review: cytokine storm syndrome: looking toward the

precision medicine era, Arthritis Rheum. 69 (2017) 1135–1143.

[38] M. Shimizu, Y. Nakagishi, N. Inoue, M. Mizuta, G. Ko, Y. Saikawa, et al., Interleukin-18 for predicting the development of macrophage activation syndrome in systemic juvenile idiopathic arthritis, Clin. Immunol. 160 (2015) 277–281.

[39] J. Bleesing, A. Prada, D.M. Siegel, J. Villanueva, J. Olson, N.T. Ilowite, et al., The diagnostic significance of soluble CD163 and soluble interleukin-2 receptor alpha-chain in macrophage activation syndrome and untreated new-onset systemic juvenile idiopathic arthritis, Arthritis Rheum. 56 (2007) 965–971.

[40] A. Takahashi, M. Mori, T. Naruto, S. Nakajima, T. Miyamae, T. Imagawa, et al., The role of heme oxygenase-1 in systemic-onset juvenile idiopathic arthritis, Mod. Rheumatol. 19 (2009) 302–308.

[41] Q. Zhou, G.S. Lee, J. Brady, S. Datta, M. Katan, A. Sheikh, et al., A hypermorphic missense mutation in PLCG2, encoding phospholipase Cgamma2, causes a dominantly inherited autoinflammatory disease with immunodeficiency, Am. J. Hum. Genet. 91 (2012) 713–720.

[42] M.J. Ombrello, E.F. Remmers, G. Sun, A.F. Freeman, S. Datta, P. Torabi-Parizi, et al., Cold urticaria, immunodeficiency, and autoimmunity related to PLCG2 deletions, N. Engl. J. Med. 366 (2012) 330–338.

[43] P. Yu, R. Constien, N. Dear, M. Katan, P. Hanke, T.D. Bunney, et al., Autoimmunity and inflammation due to a gain-of-function mutation in phospholipase C gamma 2 that specifically increases external Ca2+ entry, Immunity 22 (2005) 451–465.